Photo-Excited Surface Dynamics from Massively Parallel Constrained-DFT Calculations

A. Lücke, T. Biktagirov, A. Riefer, M. Landmann, M. Rohrmüller, C. Braun, S. Neufeld, U. Gerstmann, and W.G. Schmidt

Abstract Constrained density-functional theory (DFT) calculations show that the recently observed optically induced insulator-metal transition of the In/Si(111)(8×2)/(4×1) nanowire array (Frigge et al., Nature 544:207, 2017) corresponds to the non-thermal melting of a charge-density wave (CDW). Massively parallel numerical simulations allow for the simulation of the photo-excited nanowires and provide a detailed microscopic understanding of the CDW melting process in terms of electronic surface bands and selectively excited soft phonon modes. Excited-state molecular dynamics in adiabatic approximation shows that the insulator-metal transition can be as fast as 350 fs.

1 Introduction

Phase transitions between equilibrium states of matter as function of temperature, pressure, magnetics fields, etc. are ubiquitous. Typically, their direct atomic scale observation is not possible and they are described in terms of statistical ensembles and phenomenological models, see, e.g. [1]. For both scientific as well as technological reasons, however, it is interesting to learn how phase transitions occur at the atomic scale, at what speed they evolve, and how they can be driven. In this context, the ordered array of In nanowires that self-assemble at the Si(111) surface—first described in 1965 [2]—is a particularly intriguing example. It is an extensively studied model system for phase transitions in quasi one-dimensional systems [3]: At around 120 K a charge-density wave forms and the metallic In/Si(111)(4×1) zigzag-chain structure, stable at room temperature, transforms to an insulating (8×2) In-hexagon reconstruction [4–8]. Adsorbates, depending on their species, either decrease [9] or increase the critical temperature T_C [10]. This indicates that the charge-density wave formation is very sensitive to external perturbations [11]. In fact, it has been shown that a 50 fs laser pulse with 1.55 eV photons converts the low-temperature (8×2) phase into the room-temperature (4×1) structure even at

A. Lücke • T. Biktagirov • A. Riefer • M. Landmann • M. Rohrmüller • C. Braun • S. Neufeld • U. Gerstmann • W.G. Schmidt (✉)
Lehrstuhl für Theoretische Materialphysik, Universität Paderborn, 33095 Paderborn, Germany
e-mail: W.G.Schmidt@upb.de

W.E. Nagel et al. (eds.), *High Performance Computing in Science and Engineering '17*, https://doi.org/10.1007/978-3-319-68394-2_9

30 K, i.e., far below the phase transition temperature T_C [12, 13]. Subsequently to the laser excitation, the In nanowires are trapped for several hundred picoseconds in a metallic metastable state corresponding to a supercooled liquid. The CDW melting is clearly not related to surface heating effects as proven by surface temperature measurements [12]. The aim of the present study consists in the elucidation of the non-thermal processes that lead to the CDW melting.

2 Methodology

To this aim, we use DFT within the local-density approximation as implemented in the QUANTUM ESPRESSO package [14] and determine the In/Si(111)(8×2)/(4×1) ground- and excited-state atomic and electronic structure. The surface is modeled using periodic boundary conditions within a supercell that contains three bilayers of silicon, the bottom layer of which is saturated with hydrogen. Norm-conserving pseudopotentials in conjunction with a plane-wave basis set limited by a cutoff energy of 50 Ry are employed to describe the electronic structure. A 2×8×1 Monkhorst-Pack mesh [15] is used for Brillouin zone (BZ) sampling. Constrained DFT [16] is used to calculate excited-state potential energy surfaces (PESs) and for performing ab initio molecular dynamics (AIMD) within the adiabatic approximation. Thereby the occupation numbers of the electronic states were frozen such as to describe a specific excited electron configuration. The configurations explored here are restricted to charge neutral excitations, but do not necessarily conserve momentum. This allows for modeling configurations that result from electronic relaxation including scattering processes subsequent to vertical excitations.

Most excited-state electronic configurations will decay within a few femtoseconds, owing to electron-electron, electron-phonon, electron-hole and electron-defect scattering. The quasiparticle lifetimes of electrons due to electron-electron scattering can be accessed from the imaginary part of the electronic self-energy. We performed quasiparticle calculations using the G_0W_0 approach [17] within the on-mass-shell approximation [18]. Here, the one-particle Green's function G_0 and the screened Coulomb interaction W_0 were obtained from the DFT electronic structure. Owing to the large increase in the number of possible scattering events, the lifetimes are found to decrease rapidly to a few femtoseconds for energies of more than 1 eV above or below the Fermi energy, in marked contrast to states close to the Fermi edge, cf. Fig. 1. Therefore, only the states close to the Fermi edge were used for calculating the excited-state PESs.

The present `Quantum Espresso` constrained-DFT implementation (v6.1) is restricted to a BZ sampling with only a single **k** point. This is not sufficient for systems with strongly dispersing states such as the metallic wires studied here. Therefore, the implementation was modified to allow for an arbitrary number of **k** points. For efficiency, the implementation was written to support both the

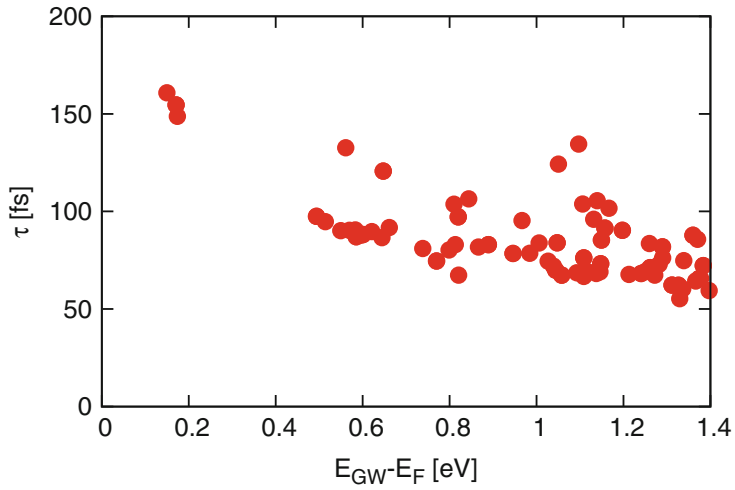

Fig. 1 Calculated lifetimes of electronic quasiparticle states in dependence on their energy relative to the Fermi level position

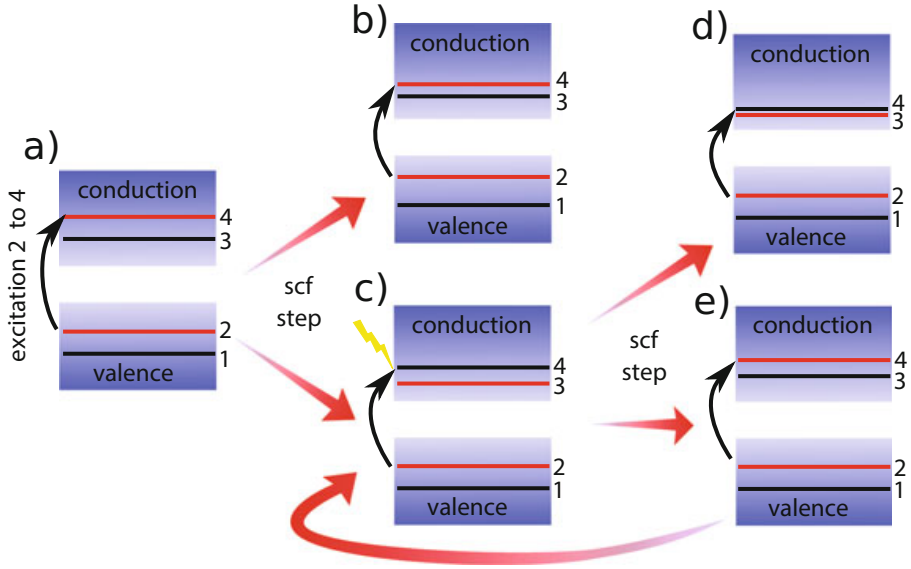

Fig. 2 Example illustrating an electronic excitation from orbital 2 to 4. The ground state is shown in (**a**), while (**b**)–(**e**) show example configurations that result from electronic relaxation upon excitation. Figures (**b**) and (**d**) represent electronically converged situations. The excitation indicated in (**d**), however, is not intended, but results from changes in the band order

parallelization with respect to **k** points (NPOOL in `Quantum Espresso`) as well as the parallelization with respect to the plane-wave coefficients. A newly defined input card within the standard input file can be used to define band and **k**-point specific occupation numbers.

Figure 2a shows exemplarily a system where an excitation of one electron from state 2 to state 4 is modeled. This excitation modifies the potential seen by the electrons and may lead to an energetic re-ordering of the orbitals. This may cause a situation where the system electronically relaxes into another excited state than

desired. Figure 2b, c show two possible configurations that may result from electron relaxation after exciting the electron as shown in Fig. 2a. Figure 2b depicts the situation that corresponds to the intended excitation. In contrast, Fig. 2c illustrates the case where the electronic relaxation led to an interchange of bands 3 and 4. If the electronic structure calculations are based on occupation numbers simply determined from the energetic order, a wrong conductance state, i.e., here the state 4 gets occupied. The originally excited (marked red) state 4 is emptied. This re-occupation of the orbitals leads to an abrupt change in the potential which may lead to two different scenarios. Either the "wrong" occupation numbers persist, as shown in Fig. 2d, or the electronic relaxation in the self-consistent field (scf) calculations swap the orbitals again, as shown in Fig. 2e. In fact, the latter scenario may result in a numerically unstable situation due to persistent charge shuffling between different electronic orbitals. Summarizing, only the electronic structure visualized in Fig. 2b corresponds to the "correctly" excited configuration, while the other situations do either not correspond to the "correct" excitation scenario and/or are numerically unstable. This problem occurs frequently for electronic states that are degenerate or close in energy. In order avoid this problem, we implemented an algorithm where the orbital symmetry of the electronic states is monitored during the scf calculations, cf. Fig. 3. This ensures that the "correct", i.e., the intended electronic

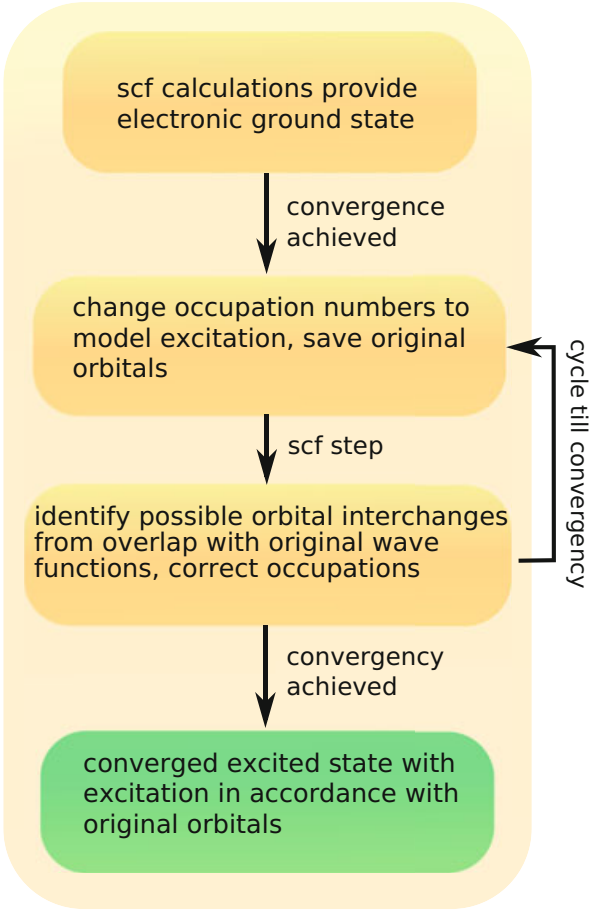

Fig. 3 Program flow in order to guarantee a convergence to the desired excited state

excitation is modeled in the constrained-DFT calculations and used, e.g., for the AIMD calculations.

In detail, we start by determining the electronic ground state. The ground-state orbitals are stored after they are numerically converged. At the same time, the occupation numbers are changed in order to describe the specific photo-excitation which needs to be modeled. Subsequently, the overlap with the stored ground-state wave functions is used to monitor the orbital symmetry of the wave functions updated during the scf cycles. This allows to choose the occupation numbers in such a way that they correctly describe the modeled excitation, even if changes in the energetic ordering of the states occur.

As mentioned above, our implementation allows for a variety of customizable parallelization schemes. In particular, parallelization (and data distribution) over **k** points as well as parallelization (and data distribution) over plane wave coefficients can to be used at the same time on massively parallel systems such as the Cray XC40 (Hazel Hen). This leads already to a high computational efficiency. However, the calculations can be sped up by an additional, third parallelization. Thereby we calculate the excited-state potential energy surface (PES) not point by point, but simultaneously for all reaction coordinates in parallel.

The performance of the Cray XC40 in combination with the mentioned parallelization strategies has been tested and optimized for the indium nanowire system within a (8×2) surface unit cell, containing 640 electrons. The computational techniques rely on mathematical libraries, in particular the Linear Algebra Package `LAPACK` or its distributed-memory implementation `ScaLAPACK`. The calculations discussed here have been performed with `ScaLAPACK`. For the (excited-state) PES calculations ten sets of reaction coordinates were calculated in parallel. The red line in Fig. 4 shows the results for taking additionally only `Quantum Espresso`'s basis parallelization (NPOOL=1) into account which distributes the plane-wave expansion coefficients across the cores. It turns out that this parallelization is only meaningful for a number of cores of the order of about 1000.

Since `Quantum Espresso` supports additionally also a parallelization over **k** points (NPOOL $>$ 1), this strategy has also been tested on Hazel Hen (cf. Fig. 4). NPOOL specifies thereby the number of **k** points that are treated in parallel. Inside a group of cores sharing the work for an individual **k** point, the other two parallelization strategies mentioned above still apply. It can be seen that the **k**-point parallelization leads to a notable saving of computation time with increasing number of cores. Especially for more than 1000 cores the **k** parallelization is mandatory to reduce the overhead caused by an increasing `MPI` communication. We find that this approach allows for the extension of the roughly linear scaling up to 10,000 cores for NPOOL $= 8$.

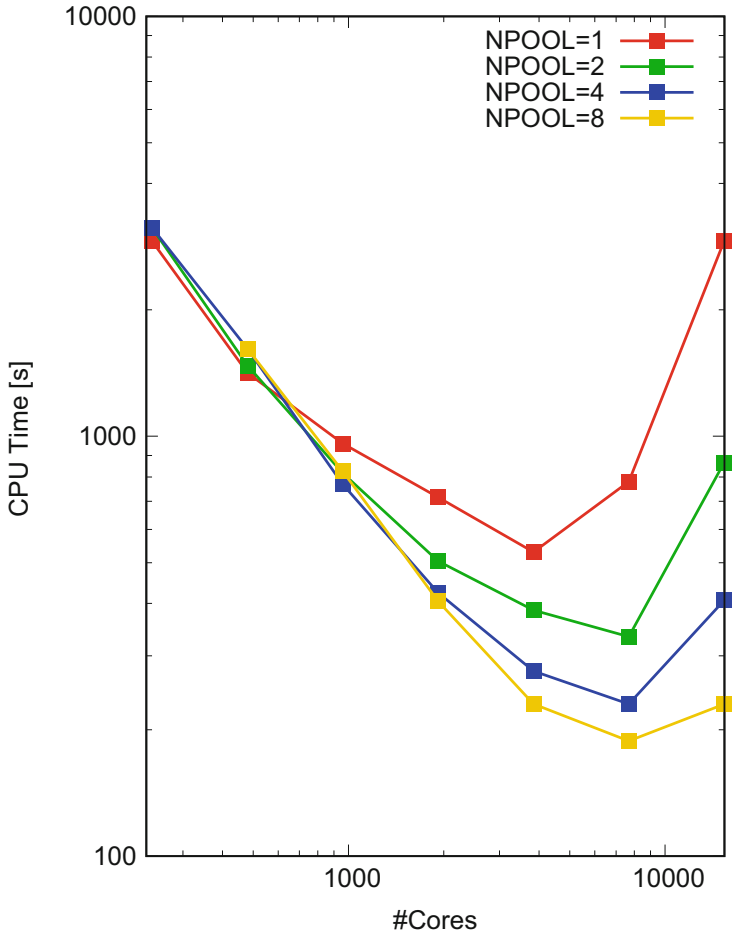

Fig. 4 CPU time on the HLRS Cray XC40 for the self-consistent calculation of the In/Si(111)(8×2) surface for various parallelization schemes. See text for details

3 Results

The photon energy used to trigger the phase transition equals 1.55 eV [12, 13]. This allows for exciting a far larger number of electronic configurations than are computationally accessible. However, not all of these configurations are long-lived enough to drive the phase transition. Their lifetimes decrease rapidly to only tens of femtoseconds with increasing distance from the Fermi energy E_F, see Fig. 1. We therefore focus on the two highest occupied (H,H−1) and the two lowest unoccupied (L,L+1) electron state of the In/Si(111)(8×2) band structure (cf. Fig. 5a) that are long-lived in the calculations and thus suitable candidates to drive the transition. These states with strong dispersion along the CDW direction correspond to strongly In-localized surface states [8].

In a second step, various excited-state PESs for charge neutral combinations between electrons in L, L+1 and holes in H, H-1 were calculated by performing constrained-DFT calculations for geometries along the minimum energy path along the (8×2) ⟶ (4×1) phase change. Thereby we sampled the surface Brillouin zone

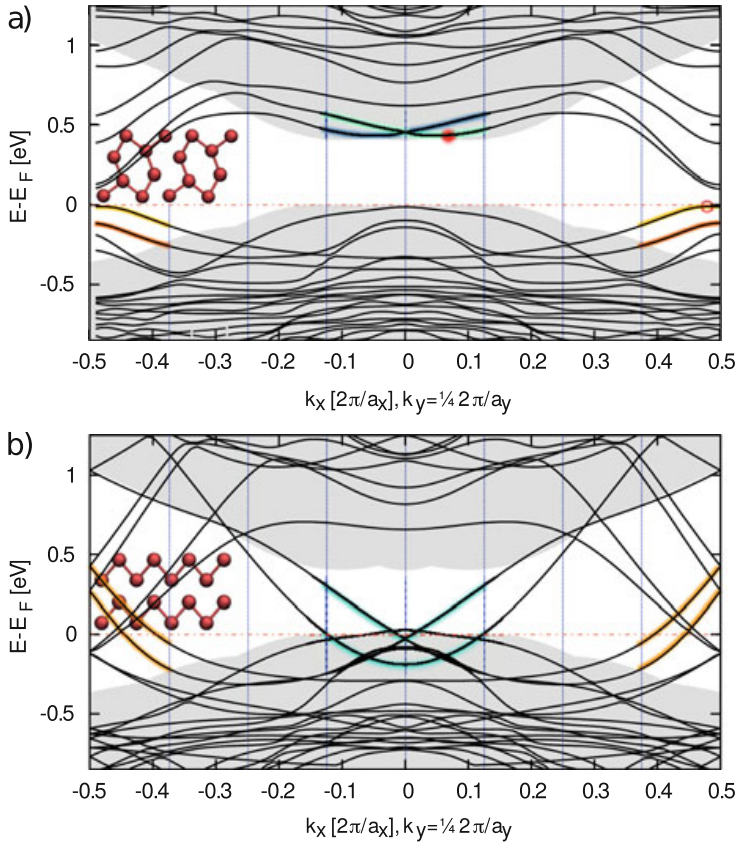

Fig. 5 (**a**) Calculated band structure of In/Si(111)(8×2) along a line within the SBZ. Blue vertical lines denote the segments used to model excitations. Exemplary a L_5;H_8 excitation is indicated. (**b**) Calculated band structure of In/Si(111)(4×1) along the same line as above

(SBZ) separately for electrons and holes using eight segments as shown in Fig. 5. Relevant examples of excited-state PESs are shown in Fig. 6 (lhs) in dependence on the generalized reaction coordinate. The calculated ground-state PES has its minimum at the (8×2) phase, separated from the metastable (4×1) structure by a distinct energy barrier of about 40 meV.

The (8×2) structure corresponds to the global minimum also for a number of excited-state PESs. This concerns, for example, the momentum conserving excitations H_1;L_1, H_2;L_2, H_3;L_3, and H_4;L_4. These excitations, however, decrease the energy difference between the (8×2) and (4×1) phases, and for even stronger excitations such as $H_{1,8}$;$L_{1,8}$ and $H_{2,7}$;$L_{2,7}$ the respective stability is even reverted, i.e., the (4×1) phase gets more stable than the (8×2) structure. Still, these excitations will not necessarily lead to a CDW melting, as there is an energy barrier separating the insulating and the metallic phase. This energy barrier disappears, however, for specific non-momentum conserving excitations such as $H_{1,8}$;$L_{4,5}$, $H_{1,8}$;$L{+}1_{4,5}$ (altogether 0.5 electron excited) or $H_{1,8}H{-}1_{1,8}$;$L_{4,5}L{+}1_{4,5}$ (altogether 1 electron excited). Obviously, excitations that combine electrons in the lowest unoccupied surface states at the SBZ center with holes residing in the uppermost valence state at the SBZ boundary are particularly prone to cause a insulator-metal transition.

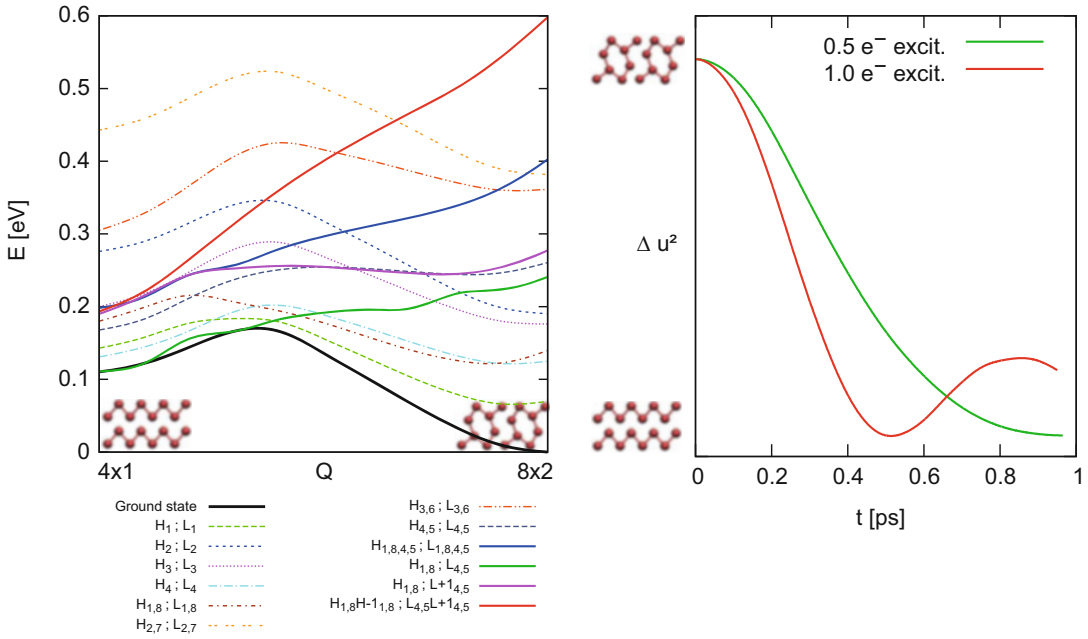

Fig. 6 (Left) Calculated ground- and excited-state potential energy surfaces vs the generalized reaction coordinate of the (8×2) ⟶ (4×1) phase transition. The numbers denotes the band structure segments indicated in Fig. 5 numbered from the left, i.e. H_1; L_1 denotes an excited state with hole in H in segment 1 and electron in L in segment 1. (Right) Calculated time evolution of the structural deviation between the (8×2) and (4×1) phases obtained from AIMD for two different excitation strengths (corresponding to the green and red solid lines lhs)

We mention that the energetics of multiple excitations composed of several single excitations cannot simply be decomposed in the excitation of the latter. As an example we show in Fig. 6 (lhs) the $H_{1,4,5,8}$;$L_{1,4,5,8}$ excitation, the PES of which obviously is not given by the sum of the $H_{1,8}$;$L_{1,8}$ and $H_{4,5}$;$L_{4,5}$ PESs.

The above analysis shows that in particular emptying/occupying the In-related valence/conduction states at the SBZ boundary/center is likely to drive the phase transition. The corresponding surface bands, highlighted yellow and orange/green and blue, respectively, in Fig. 5, are known to couple strongly to the two soft In-localized surface phonons that—in combination—describe the structural deformation characteristic for the (8×2) ⟶ (4×1) phase transition [4, 7, 19, 20]: The In-chain shear phonon mode at about 18/19 cm^{-1} lower the L and L+1 bands below the Fermi energy, while the the hexagon rotary mode at 27 cm^{-1} lifts the H and H-1 states above the Fermi level [7, 21]. The corresponding band-structure energy changes rationalize the steep PESs calculated here for the $H_{1,8}$;$L_{4,5}$ and $H_{1,8}$H-$1_{1,8}$;$L_{4,5}$L+$1_{4,5}$ excitations.

The coupling of these phonons, which were also detected by Raman spectroscopy [22], to the corresponding electronic states can be understood in terms of In-In bond formation: The L_4 and L_5 orbital characters are shown in Fig. 7. These states correspond to an In-In bond across parallel In-In zigzag chains. Electronic occupation of these bonds results in forces that exert an attractive interaction between the respective In atoms and excite the In-chain shear phonon mode.

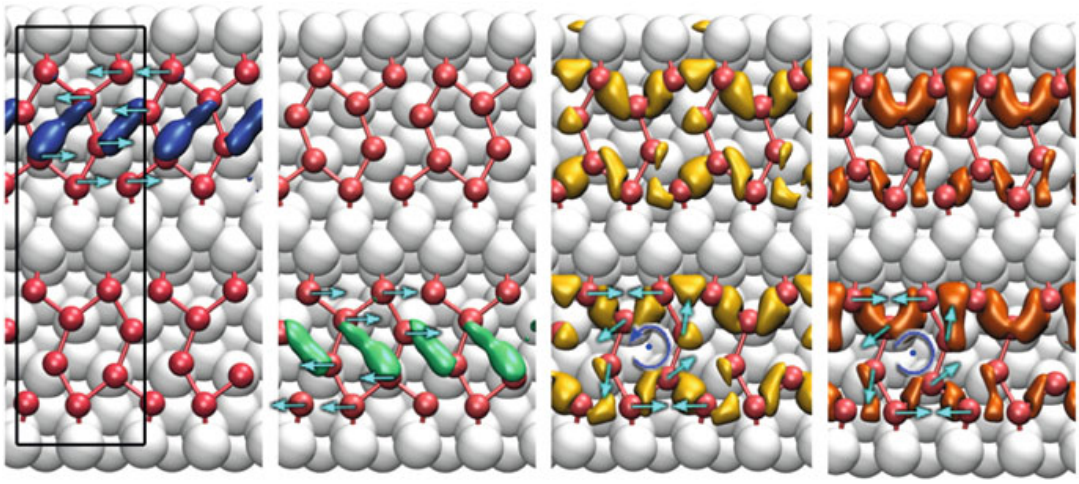

Fig. 7 Atomic structure of the In/Si(111)(8×2) surface. Dark/light balls indicate In/Si atoms. Isosurfaces indicates the orbital character of L_4, L_5, H_1, and H_8 (color coding corresponds to band structure in Fig. 5a). Arrows indicate the eigenvectors of the shear and rotary phonon modes excited upon optical excitation

Correspondingly, H_1 and H_8 are related to In hexagon bonds as well as bonds between the outermost In chain atoms, cf. Fig. 7. Emptying these bonds will prolong the corresponding In-In distances and excite the rotary phonon. The combined action of rotary and shear phonons, very effectively exited by the $H_{1,8}$;$L_{4,5}$ electronic configuration, transforms the insulating (8×2) CDW into the metallic (4×1) phase [4, 7, 19, 20]. The time scale for an optically driven phase transition can thus be expected to be set by the period of exactly these phonon modes which are known to facilitate the (8×2) ⟶ (4×1) phase change.

After having identified the driving force and the atomistic mechanism for the CDW melting, we address in a third step the time dynamics of the corresponding structural modification. For this purpose, energy conserving AIMD simulations were performed in adiabatic approximation, starting from two different electronically excited-state configurations. Specifically, we start from the $H_{1,8}$;$L_{4,5}$ (altogether 0.5 electron excited) as well as the $H_{1,8}H\text{-}1_{1,8}$;$L_{4,5}L{+}1_{4,5}$ configuration (altogether 1 electron excited), corresponding to the solid green and red PES shown in Fig. 6 (lhs), respectively. The calculated time-dependent structural deviation between the (8×2) and (4×1) phases is shown in Fig. 6 (rhs). Corresponding to the larger gradient of the PES excitation involving one electron compared to the half-electron excitation, the phase change in the former case occurs nearly twice as fast. In fact, in case of the one-electron excitation the CDW melting occurs with a time constant of 350 fs. This is about one quarter of the periods of the equilibrium rotational and shear phonon modes discussed above, T_{rot} = 1.2 ps and T_{shear} = 1.8 ps [7], respectively.

The AIMD shows that the energy of the excited electron configuration is at first primarily transformed to the In structural degrees of freedom, exciting the shear and rotary phonon modes. However, the velocity components soon equilibrate, first

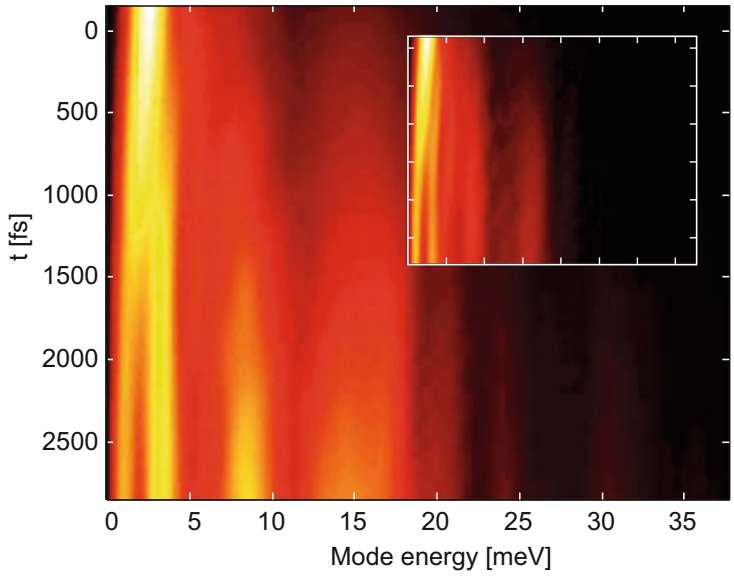

Fig. 8 Calculated distribution of the kinetic energy among the surface phonon modes of the In/Si(111) surface during the (8×2) ⟶ (4×1) phase transition. Only In related surface phonon modes are considered in the inset

among all the In chain atoms and secondly among In and Si substrate atoms. About 20% of the kinetic energy is dissipated into the Si substrate after 1 ps. This can be seen in Fig. 8, where we show the distribution of the kinetic energy among the surface phonon modes of the In/Si(111) surface. The system gets trapped in the metastable (4×1) phase and cannot revert to the (8×2) ground state.

The present calculations clearly show a non-thermal melting of the CDW. A very recent macroscopic theory analysis for bulk material [23] suggests that non-thermal melting is restricted to materials having an anomalous phase diagram like ice characterized by $dT_C/dp < 0$, where T_C is the melting temperature and p is pressure. Interestingly, this condition is fulfilled for the present nanowire system: Density-functional calculations of the phase transition temperature T_C in dependence on the substrate lattice constant show indeed the respective anomaly [24]. Also the number of electrons that need to be excited for the phase transition to occur, about 5% of the In chain valence electrons, is similar to various bulk systems, see discussion in [23].

4 Conclusions

In summary, first-principles calculations were performed in order to rationalize the optically induced insulator-metal transition of the Si(111) substrate-stabilized In nanowire array. (1) It is found that the In-related surface states within the Si fundamental gap are long-lived with respect to electron-electron scattering. (2) Some photo-excited configurations involving these states, in particular electrons in empty zone-center surface states as well as holes in the uppermost In states at the

Brillouin zone boundary give rise to a potential energy surface that has its minimum at the metallic phase and allows for a barrierfree transition. (3) The energy gain realized upon relaxing these electronic states excites directly the shear and rotary phonon modes that transform between the insulating and metallic nanowire phases. (4) The phase transition may be completed within less than one picosecond. Thereby stronger electronic excitations result in shorter transition times.

Acknowledgements The Deutsche Forschungsgemeinschaft is acknowledged for financial support (FOR1700 and FOR1405). We thank the Paderborn Center for Parallel Computing (PC^2) and the Höchstleistungs-Rechenzentrum Stuttgart (HLRS) for grants of high-performance computer time. Images of molecular structures were prepared using `VMD` [25] and the `tachyon` renderer.

References

1. P.M. Chaikin, T.C. Lubensky, *Principles of Condensed Matter Physics* (Cambridge University Press, Cambridge, 2000)
2. J.J. Lander, J. Morrison, J. Appl. Phys. **36**, 1706 (1965)
3. P.C. Snijders, H.H. Weitering, Rev. Mod. Phys. **82**(1), 307 (2010)
4. C. Gonzalez, F. Flores, J. Ortega, Phys. Rev. Lett. **96**, 136101 (2006)
5. A.A. Stekolnikov, K. Seino, F. Bechstedt, S. Wippermann, W.G. Schmidt, A. Calzolari, M. Buongiorno Nardelli, Phys. Rev. Lett. **98**, 026105 (2007)
6. S. Chandola, K. Hinrichs, M. Gensch, N. Esser, S. Wippermann, W.G. Schmidt, F. Bechstedt, K. Fleischer, J.F. McGilp, Phys. Rev. Lett. **102**(22), 226805 (2009)
7. S. Wippermann, W.G. Schmidt, Phys. Rev. Lett. **105**, 126102 (2010)
8. U. Gerstmann, N.J. Vollmers, A. Lücke, M. Babilon, W.G. Schmidt, Phys. Rev. B **89**, 165431 (2014)
9. S.V. Ryjkov, T. Nagao, V.G. Lifshits, S. Hasegawa, Surf. Sci. **488**, 15 (2001)
10. H.W. Yeom, D.M. Oh, S. Wippermann, W.G. Schmidt, ACS Nano **10**, 410 (2016)
11. W.G. Schmidt, M. Babilon, C. Thierfelder, S. Sanna, S. Wippermann, Phys. Rev. B **84**, 115416 (2011)
12. S. Wall, B. Krenzer, S. Wippermann, S. Sanna, F. Klasing, A. Hanisch-Blicharski, M. Kammler, W.G. Schmidt, M.H. von Hoegen, Phys. Rev. Lett. **109**, 186101 (2012)
13. T. Frigge, B. Hafke, T. Witte, B. Krenzer, C. Streugebühr, A. Samad Syed, V. Miksic Trintl, P. Avigo, I. Zhou, M. Ligges, D. von der Linde, U. Bovensiepen, M. Horn-von Hoegen, S. Wippermann, A. Lücke, S. Sanna, U. Gerstmann, W.G. Schmidt, Nature **544**, 207 (2017). https://doi.org/10.1038/nature21432
14. P. Giannozzi, S. Baroni, N. Bonini, M. Calandra, R. Car, C. Cavazzoni, D. Ceresoli, G.L. Chiarotti, M. Cococcioni, I. Dabo, A. Dal Corso, S.D. Gironcoli, S. Fabris, G. Fratesi, R. Gebauer, U. Gerstmann, C. Gougoussis, A. Kokalj, M. Lazzeri, L. Martin-Samos, N. Marzari, F. Mauri, R. Mazzarello, S. Paolini, A. Pasquarello, L. Paulatto, C. Sbraccia, S. Scandolo, G. Sclauzero, A.P. Seitsonen, A. Smogunov, P. Umari, R.M. Wentzcovitch, J. Phys. Condens. Matter **21**(39), 395502 (2009)
15. H.J. Monkhorst, J.D. Pack, Phys. Rev. B **13**(12), 5188 (1976)
16. P.H. Dederichs, S. Blügel, R. Zeller, H. Akai, Phys. Rev. Lett. **53**, 2512 (1984)
17. W.G. Aulbur, L. Jonsson, J.W. Wilkins, Quasiparticle calculations in solids, in *Solid State Physics: Advances in Research and Applications*, vol. 54 (Academic, San Diego, 2000), p. 1
18. P. Echenique, J. Pitarke, E. Chulkov, A. Rubio, Chem. Phys. **251**(1) (2000)
19. S. Riikonen, A. Ayuela, D. Sanchez-Portal, Surf. Sci. **600**, 3821 (2006)

20. C. González, J. Guo, J. Ortega, F. Flores, H.H. Weitering, Phys. Rev. Lett. **102**(11), 115501 (2009)
21. W.G. Schmidt, S. Wippermann, S. Sanna, M. Babilon, N.J. Vollmers, U. Gerstmann, Phys. Stat. Sol. (b) **249**, 343 (2012)
22. K. Fleischer, S. Chandola, N. Esser, W. Richter, J.F. McGilp, Phys. Rev. B **76**, 205406 (2007)
23. H. Hu, H. Ding, F. Liu, Sci. Rep. **5**, 8212 (2015)
24. M. Babilon, Phasenübergangsstabilität von Substrat-gestützten Indiumnanodrähten. Master's thesis, Universität Paderborn, 2013
25. W. Humphrey, A. Dalke, K. Schulten, J. Mol. Graph. **14**(1), 33 (1996)